Astron. Astrophys. 66, 13—29 (1978)

ASTRONOMY AND ASTROPHYSICS

Structure and Kinematics of H_2O Sources in Clusters of Newly-formed OB Stars

R. Genzel[1], D. Downes[1], J. M. Moran[2], K. J. Johnston[3], J. H. Spencer[3], R. C. Walker[4], A. Haschick[4], L. I. Matveyenko[5], L. R. Kogan[5], V. I. Kostenko[5], B. Rönnäng[6], O. E. H. Rydbeck[6] and I. G. Moiseev[7]

[1] Max-Planck-Institut für Radioastronomie, Auf dem Hügel 69, D-5300 Bonn 1, Federal Republic of Germany
[2] Center for Astrophysics, Harvard College Observatory and Smithsonian Astrophysical Observatory, 60 Garden Street, Cambridge, Mass. 02138, USA
[3] E. O. Hulburt Center for Space Research, Naval Research Laboratory, Washington, D.C. 20375, USA
[4] Department of Physics and Research Laboratory of Electronics, Massachusetts Institute of Technology, Cambridge, Mass. 02139, USA
[5] Institute for Space Research, USSR Academy of Sciences, Profsojuznaya 88, 117810 Moscow, USSR
[6] Onsala Space Observatory, S-43034 Onsala, Sweden
[7] Crimean Astrophysical Observatory, USSR Academy of Sciences, Simeis, Crimea, USSR

Received October 18, 1977

Summary. We report VLBI observations at 22 GHz of 12 galactic water vapor sources in regions of star formation. The improved sensitivity in this experiment permitted the determination of relative positions to a few milli arc sec for maser lines $\geqq 10$ Jy. In all of the sources the H_2O lines are concentrated in "centers of activity" of size $\sim 10^{16}$ cm. In the Orion nebula, the dominant H_2O, OH and SiO source is coincident in position with the strong compact IR source, IRc4 in the Kleinmann-Low nebula. We think that each "center of H_2O activity" should be identified with the envelope of a young, massive star. The number of "centers" probably indicates that in Orion-KL, W3-IRS 5 and W49 N, clusters of 2 to 10 OB stars are currently being formed in regions of size $\sim 3\ 10^{17}$ cm. The H_2O sources W51 M and NGC 7538 S appear to be associated with single stars. The spatial distribution of the H_2O velocities in these latter two sources suggests that the stellar envelopes are expanding and rotating, and shaped like disks. Strong H_2O emission comes preferentially from the line of sight to the star and the edges of the disk. Weaker, "high velocity" features may be blown out at the poles. Alternatively, the "high velocity" fragments could be shot out through transient holes or tunnels in circumstellar shells. The examples of Orion-KL, W51 S, and possibly W49 N, show that there is H_2O emission at the same position and at the same velocity as OH maser radiation at 1665 MHz.

Key words: very long baseline interferometry — H_2O masers — star formation — circumstellar shells

The strong H_2O sources in regions of star formation show two different types of line radiation. Strong, *low velocity emission* occurs at about the radial velocities of the associated molecular clouds or H II regions, often with a symmetrical arrangement of lines or line groups over a range of $\sim \pm 15$ km s^{-1}. Weak, *high velocity features* are spread ± 15 to ± 250 km s^{-1} around the low velocity emission. Recent VLBI and single-dish observations show that the low velocity masers tend to cluster in "centers of activity" of size 10^{16} cm, which are sometimes surrounded by a larger zone containing the weak, high velocity features (Walker et al., 1977; Genzel and Downes, 1977a).

The high luminosities of the H_2O lines (typically 10^{-4} $L_\odot$ in a 50 kHz-wide line at 22 GHz) require powerful pump sources.

The symmetrical patterns in the spectra and the VLBI observations of "centers of activity" suggest that the material is in ordered motion in disks or shells around massive stars. The H_2O masers thus promise to be sensitive probes of the motions of this circumstellar material. We present here a further discussion of these ideas, with the help of new VLBI results of improved sensitivity and positional accuracy for twelve galactic H_2O sources.

Observations and Data Reduction

The observing dates and the instrumental parameters of the participating stations are given in Table 1. The data were recorded with the NRAO Mark II video tape recording system (Clark, 1973). The coherence times at 22 GHz, defined as the integration time for which the fringe amplitude falls to half of its true value, were 30 and 600 s for data taken with rubidium and hydrogen maser standards respectively.

The data were reduced on the Mark II VLBI processor of the NRAO in Charlottesville, Virginia. The mapping technique was the standard fringe rate method (Moran, 1976). The initial output of the processor is a cross-correlated spectrum of 128 channels covering 2 MHz, with a velocity resolution of 0.34 km s^{-1}. The data are then coherently averaged over records of length 2–15 s, depending on the spatial field of view required. A strong spectral feature is selected as a reference, and

Send offprint requests to: R. Genzel

Table 1. Instrumental Parameters for the Individual VLB Stations

Station	Telescope Diameter (m)	System Temp. in Zenith (K)	Aperture Efficiency	S/T_a = Response for point source in the Zenith (Jy/K)	Type of Time Standard	Type of Receiver	Observing Dates [c]
Simeis, Crimea	22	100	0.38	19	H-maser	maser	4- 6 Dec. 1976 (LC) 27-28 Feb. 1977 (LC)
Onsala	20	110	0.50 [a]	18	H-maser	maser	27-28 Feb. 1977 (LC)
Effelsberg	100	160	0.25 [b]	2.2	Rubidium	cooled paramp	27-28 Feb. 1977 (LC)
Haystack	37	120	0.17	17	H-maser	maser	4- 6 Dec. 1976 (RC, LC) 27-28 Feb. 1977 (LC)
Maryland Point	26	1500	0.43	13	H-maser	mixer	4- 6 Dec. 1976 (NS)

a) Includes attenuation by radome; tentative value

b) For inner 80-m diameter

c) Polarization is given in parentheses (RC, LC = right, left circular, NS = linear north-south)

its phase is subtracted from those of the other line features. This procedure makes it possible to coherently integrate for longer than the coherence time of the interferometer clocks. A second Fourier transform of 60 such records gives the unnormalized fringe visibility as a function of fringe rate and spectral frequency, that is, radial velocity (see Fig. 5 as an example).

The fringe rate, relative to that of the reference, is determined for the strongest feature in each frequency channel, with the simplifying approximation that there is only *one* H_2O feature per channel. The mapping program then analyses the change of this relative fringe rate with hour angle and fits to it a positional offset (θ_x, θ_y), in R.A. and Dec., from the reference feature (Johnston et al., 1971).

The theoretical accuracy with which a relative position can be determined is ~ 0.01 milli arc sec for a 200 Jy line and a typical baseline in this experiment. However, systematic errors and approximations in the processing and post-processing reduction limit the positional accuracy in practice to about 1 milli arc sec. The errors quoted in the tables and figures in this paper are twice the positional uncertainties derived from the least-squares fitting in the mapping program. This seems to be a realistic error estimate, from a comparison of fringe-rate maps made in the past six years.

The minimum detectable line flux in this experiment was ~ 10 Jy. There has thus been an improvement in positional accuracy and sensitivity of a factor of ~ 5 over most previous H_2O-line VLBI experiments.

Results on Individual Sources

W3-IRS 5

The compact infrared object W3-IRS 5 has H_2O emission with a complicated spatial structure. The plot of fringe rate vs. spectral frequency reveals that there are often several features at a given radial velocity. Table 2 gives the relative H_2O positions measured in February 1977, and Figure 1 compares them with positions obtained with the Hat Creek interferometer (triangles; Forster et al., 1977) and in VLBI maps of January 1974 (crosses, Moran et al., 1978) and March 1975 (squares, Walker, 1977). For the few features common to all four measurements, the relative positions coincide to within the errors of 0".1.

IRS 5 consists of at least three centers of H_2O activity, indicated roughly by the dashed boundaries in Figure 1. These three "centers" have similar H_2O line intensities, and overlap in radial velocity, with a mean of -40 km s^{-1}. IRS 5 has also been resolved in the infrared, into a double source with a separation of 1" (see Wynn-Williams, 1976). We suspect that the H_2O lines and infrared emission both originate in the same circumstellar shells, and that IRS 5 is a young star cluster comparable in linear size with the Kleinmann-Low nebula in Orion.

W3(OH)

The new results (Fig. 2 and Table 3) confirm the 2" east-west distribution of H_2O masers seen in earlier interferometric measurements (Moran et al., 1973; Mader et al., 1975, 1977; Forster et al., 1977). As in the past, the center of activity at the east radiates $>90\%$ of the H_2O luminosity, and is presumably the location of a massive star.

The line at -48.1 km s^{-1} which has dominated the spectrum of W3(OH) since its discovery, was a *double source* in December 1976 and February 1977 (cf. Fig. 3). The double consisted of two components of nearly

Table 2. Relative intensities and positions of H_2O features in W3-IRS5 in February 1977

V_{LSR} (km s^{-1})	Average Relative Intensity[a] (per cent)	Relative Position[b] θ_x (R.A.) (milli arc sec)	θ_y (Dec.) (milli arc sec)
-33.9	30	+423 ± 8	+ 273 ± 6
-34.6	100	+446 ± 20	-1614 ± 50
-35.8	100	- 71 ± 2	- 539 ± 3
-35.8	80	+360 ± 60	+ 680 ± 200
-37.3	7	-282 ± 2	- 169 ± 3
-38.5	15	- 40 ± 3	- 36 ± 3
-39.2[c]	50	0	0
-39.6	40	-286 ± 8	+ 688 ± 6
-40.6	30	- 69 ± 20	+ 537 ± 8
-40.6	50	+ 15 ± 40	+1010 ± 300
-41.6	60	-291 ± 3	- 158 ± 4
-42.3	10	- 29 ± 100	+ 828 ± 100
-43.6	20	+329 ± 8	+ 775 ± 8
-44.3	20	-194 ± 3	- 363 ± 4
-45.1	4	+ 38 ± 20	+ 570 ± 100
-47.1	20	-282 ± 5	- 70 ± 5
-49.7	5	-161 ± 4	- 320 ± 5

a) From cross-correlation spectrum ; 100 % = 200 Jy.

b) Errors are two standard deviations.

c) Reference feature; (0,0) = $02^h21^m53.14^s \pm 0.05^s$, $+61°52'21.4'' \pm 0.4''$ (1950) (Forster et al. 1977).

equal intensity, separated by 6.3 ± 0.3 milli arc sec, (or $2.6\ 10^{14}$ cm) in position angle 1.7° east of north.

The -50.3 km s^{-1} feature in the "center of activity" indicated by the dashed ellipse in Figure 2 is of particular interest. This component flared up in May-June 1977 relative to the H_2O features at other velocities (Haschick et al., 1977). The H_2O intensity rose steeply in 4 days and then decayed slowly over 25 days to its original value. Haschick et al. conclude that the source of excitation must have been of short duration and highly directional.

A comparison of VLBI maps from 1971 onwards proves that the positions of the H_2O masers in W3(OH) have remained constant to within 0.″1 over the years. There appears to be only one real "center of activity" with several H_2O lines at different velocities; the weaker emission to the west seems to come from isolated spots, each at a single velocity. If the weak emitters are "high velocity features" associated with the center of activity, then why are they grouped in a preferential direction? It would be interesting in this context to map the other high velocity features in the spectrum of W3(OH) over the range -20 to -75 km s^{-1}, which were outside our 2 MHz observing bandwidth in these experiments.

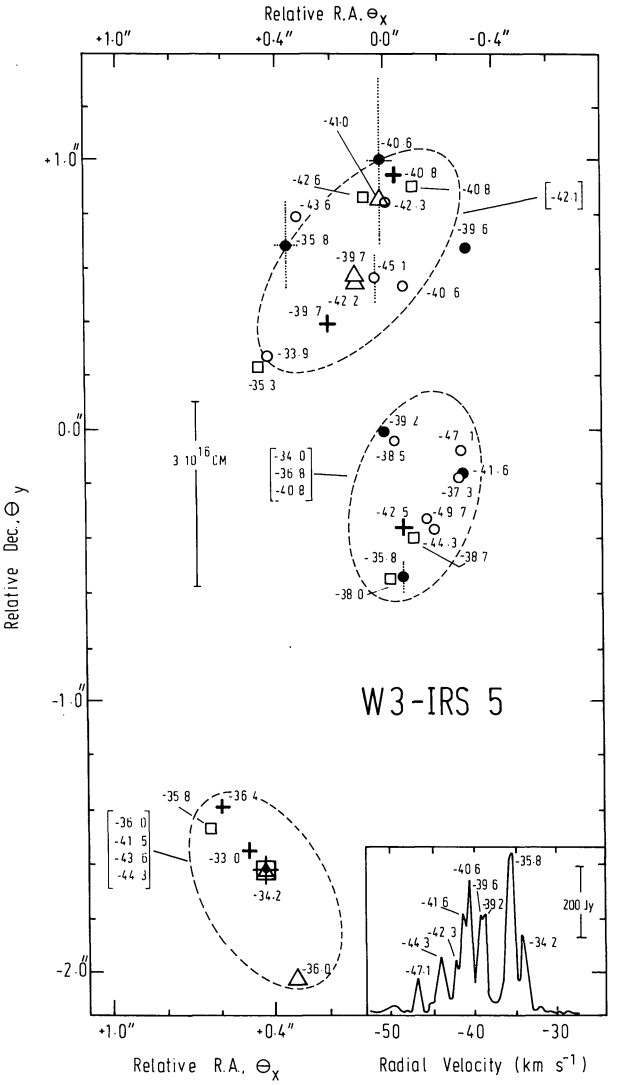

Fig. 1. Spatial distribution of the H_2O features in W 3-IRS 5 relative to the line at -39.2 km s^{-1} in February 1977 (small circles). Shaded circles indicate strong lines ($\geq$100 Jy) in the cross-correlation spectra; unshaded circles represent weaker lines. Labels are LSR velocities (km s^{-1}). Velocities in brackets are minor features found in plots of fringe rate vs. spectral frequency. Dashed ellipses denote the approximate boundaries of "centers of activity". The relative positional errors (see Table 2) are comparable with the size of the circles. Where this is not the case, errors are shown by dotted lines. Also shown are the positions of features observed in January 1974 (Moran et al., 1978; small crosses) and in March 1975 (Walker, 1977; squares). Triangles are positions measured by Forster et al. (1977). These different data were aligned on the feature at -34.2 km s^{-1}, which is common to all maps. The zero of the coordinate system is $02^h21^m53.14^s \pm 0.05^s$, $+61°52'21.4'' \pm 0.4''$ (1950), derived from the data of Forster et al. The linear scale is for an assumed distance of 3 kpc. The inset shows the single dish spectrum obtained at Effelsberg in February 1977

Orion-KL

Our new VLBI map (Fig. 4 and Table 4) has greatly improved sensitivity over previous maps, and covers all the strong, low-velocity lines. The new VLBI positions are plotted relative to the feature at 10.8 km s^{-1}. The triangles give the position of the lines at 2.4, 3.7 and 26.8 km s^{-1} (Moran et al., 1973 and Forster et al., 1978), which were not visible in February 1977. Weaker features on the plots of fringe rate vs. spectral frequency

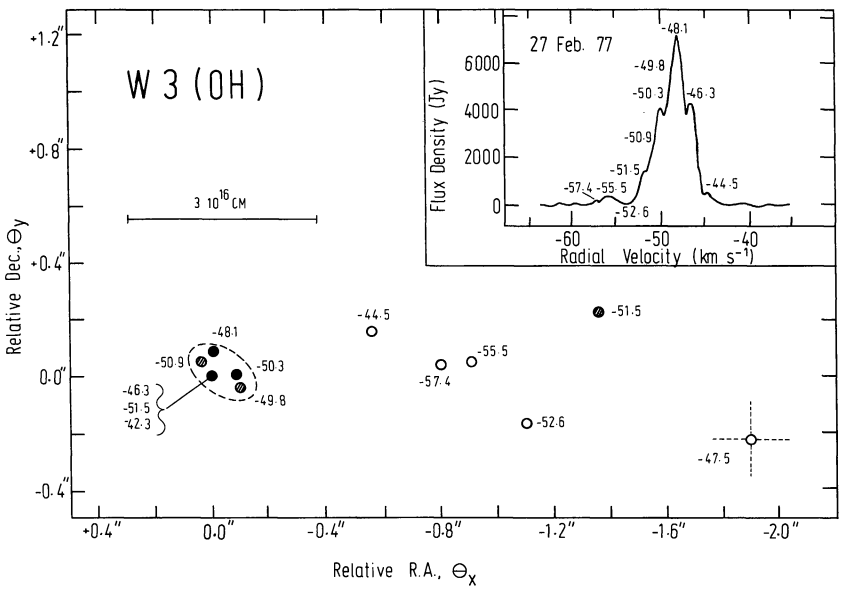

Fig. 2. Positions of H_2O masers in W3(OH) relative to the feature at -46.3 km s^{-1} in February 1977. Labels are LSR velocities in km s^{-1}. Positional uncertainties are indicated by filled circles for strong (>3000 Jy) features, shaded circles for intermediate (>1000 Jy) features, and open circles for weaker features. The dashed line indicates a possible "center of activity", which contains >90% of the H_2O luminosity in W3(OH). The zero of the coordinate system is at $02^h23^m17.30^s \pm 0.03^s$, $+61°38'57.6'' \pm 0.4''$ (1950) (Forster et al., 1977). The linear scale is for an assumed distance of 3 kpc

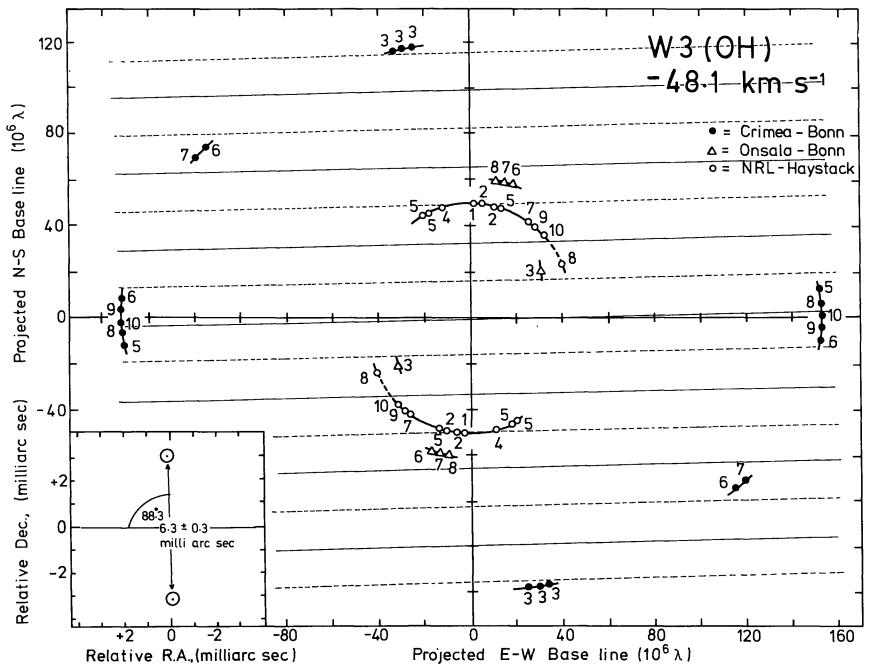

Fig. 3. Fringe visibilities of the H_2O feature at -48.1 km s^{-1} in W3(OH) in the projected baseline plane. The labels are fringe visibility $\times 10$. Only the innermost baselines are shown. The simplest interpretation of the data is a pattern of maxima and minima indicated by the horizontal lines. The Fourier transform of this pattern is a double source (inset). The two components have nearly equal intensity and are separated by 6.3 ± 0.3 milli arc sec in position angle 1.7° east of north

(Fig. 5) can be assigned to the individual centers of activity. These features are listed in brackets in the figures, but are not given in Table 4.

The large cross in Figure 4 is the position of the 1665 MHz maser lines of OH at 3.9, 7.1 and 8.6 km s^{-1} (Hansen et al., 1977). A new map by Norris (1977), with the Jodrell Bank radio-link interferometer, shows that the other strong OH lines in the range 17 to 23 km s^{-1} are ~5".5 east and 3".5 north of the position marked by the cross.

Figure 6 also shows the H_2O data, aligned with the absolute position of the feature at 10.8 km s^{-1} (Forster et al., 1978), and superimposed on the 21 μ infrared emission of the Kleinmann-Low nebula (Rieke et al., 1973; Wynn-Williams and Becklin, 1974). The large crosses mark the positions of the weak, high-velocity H_2O features mapped with the 100-m telescope (Genzel and Downes, 1977a).

Figures 4 and 6 show that the low velocity lines cluster in at least nine "centers of activity" of size 1–2 10^{16} cm, indicated by the dashed lines in the figures. Some of the "centers" appear to be elongated rather than spherical, even if these boundaries are slightly arbitrary. Error bars are not drawn in the figures,

Table 3. Relative intensities and positions of H_2O features in W3(OH)

V_{LSR} (km s^{-1})	Average Relative Intensity[a] (per cent)	Relative Positions[b] Dec. 76 (Haystack-NRL) θ_x (R.A.) (milli arc sec)	Dec. 76 (Haystack-NRL) θ_y (Dec.) (milli arc sec)	Feb. 77 (Bonn-Onsala-Crimea) θ_x (R.A.) (milli arc sec)	Feb. 77 (Bonn-Onsala-Crimea) θ_y (Dec.) (milli arc sec)
-42.3	1		--	-4 ± 8	-5 ± 6
-44.5	5	- 554 ± 30	+136 ± 50	- 564 ± 2	+151 ± 2
-46.3[c]	100	0	0	0	0
-47.5		--	--	-1900 ±180	-220 ±110
-48.1[d]	100	-1 ± 4	+ 72 ± 7	+3 ± 2	+ 85 ± 2
-49.8	30	-44 ± 40	+ 25 ± 60	-98 ± 10	-44 ± 10
-50.3	40	-55 ± 30	- 12 ± 60	-80 ± 30	0 ± 30
-50.9	30	+ 5 ± 10	+ 17 ± 20	35 ± 10	50 ± 8
-51.5	20	-1374 ± 30	+224 ± 60	-1370 ±180	--
-51.5	20	--	--	+1 ± 4	+6 ± 3
-52.6	4	--	--	-1111 ± 30	-170 ± 30
-55.5	8	- 915 ± 20	+ 80 ± 40	- 921 ± 2	+ 49 ± 2
-57.4	1	--	--	- 810 ± 6	+ 46 ± 5

a) From cross-correlation spectrum; intensities are average of spectra in Dec. 76 and Feb. 77; 100 % ≙6000 Jy.

b) Errors are two standard deviations.

c) Reference feature; (0,0) = $02^h23^m17.30^s \pm 0.03^s$, $61°38'57.6'' \pm 0.4''$ (1950) (Forster et al. 1977)

d) Double source (see text); position given here probably refers to centroid.

Table 4. Relative Intensities and Positions of H_2O Features in Orion - KL in February 1977

V_{LSR} (km s^{-1})	Average Relative Intensity[a] (per cent)	Relative Position[b] θ_x (R.A.) (milli arc sec)	θ_y (Dec.) (milli arc sec)
-6.1	0.4	- 8690 ± 70	-15920 ± 2000
-5.3	0.5	-11680 ± 20	-19500 ± 400
-4.9	1	-15060 ± 7	-17180 ± 20
-3.8	1	-15060 ± 7	-17180 ± 20
-1.7	20	-15060 ± 7	-17180 ± 20
-0.9	1	- 8370 ± 7	-12900 ± 100
0.8	2	-14390 ± 7	-24130 ± 10
1.7	4	- 4715 ± 20	- 900 ± 30
2.7	10	-14400 ± 7	-24160 ± 100
3.2	40	-12250 ± 7	-18600 ± 100
3.8	4	-14410 ± 7	-24150 ± 7
5.3	10	- 4605 ± 7	- 905 ± 20
6.5	4	-15170 ± 7	-20890 ± 150
7.6	3	-14445 ± 7	-22370 ± 7
7.6	30	-12126 ± 7	-19270 ± 40
8.3	40	-11540 ± 40	-21270 ± 200
8.9	50	-19083 ± 7	-22450 ± 60
9.9	25	+ 135 ± 7	- 25 ± 60
10.3	15	-14380 ± 7	-22400 ± 10
10.8[c]	100	0	0
11.9	10	- 570 ± 10	-23750 ± 70
12.4	10	- 570 ± 10	-23750 ± 70
14.5	1	- 9340 ± 20	-13500 ± 200
15.4	3	- 895 ± 7	- 1310 ± 60
16.2	9	-19635 ± 10	-22137 ± 50
17.0	5	-14985 ± 7	-22095 ± 10
17.6	8	-19710 ± 40	-22380 ± 200
18.3	15	-11380 ± 20	-21160 ± 400
18.8	1	-19790 ± 40	-22690 ± 800
20.5	2	-15600 ± 60	-18190 ± 1200
22.8	1	-21030 ± 80	-23190 ± 1600
24.3	2	-18750 ± 40	-22090 ± 800
24.8	20	-11070 ± 40	-21590 ± 600
25.8	8	-18690 ± 8	-22935 ± 40
27.1	95	-14648 ± 5	-19385 ± 20
27.1	30	-18700 ± 1000	-23150 ± 1000
28.1	55	-14648 ± 5	-19385 ± 20
31.3	1	-14640 ± 50	-20070 ± 800

a) From cross-correlation spectrum; 100 % ≙6000 Jy.

b) Errors are two standard deviations.

c) Reference feature; (0,0) = $05^h32^m47.58^s \pm 0.02^s$ $-05°24'09.3'' \pm 0.5''$ (1950), (Forster et al, 1978)

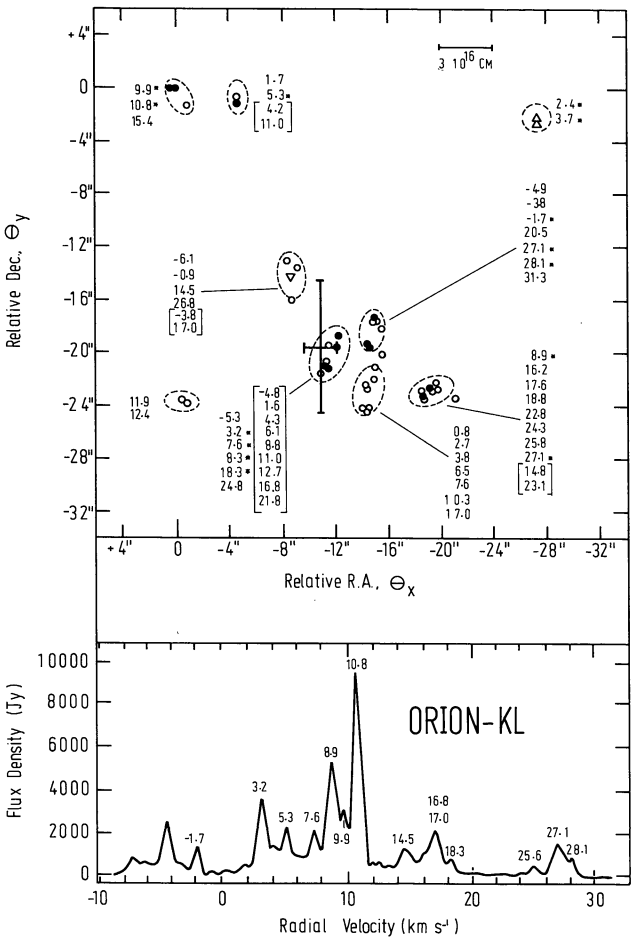

Fig. 4. VLBI positions for the low-velocity H_2O features in Orion-KL in February 1977, relative to the line at 10.8 km s^{-1}. Labels are LSR velocities in km s^{-1}. Circles indicate the main features; strong (>1000 Jy) lines are marked by asterisks and shaded circles. Weaker features on the plots of fringe rate vs. spectral frequency (cf. Fig. 5) are listed in brackets. Typical error bars (not shown) are 0".01–0".1. The lines at 2.4 and 3.7 km s^{-1} (upright triangles; Moran et al., 1973) and at 26.8 km s^{-1} (inverted triangle; Forster et al., 1978) were not visible in February 1977. Dashed lines are possible boundaries of "centers of activity". The cross marks the position of the OH features at 3.9, 7.1 and 8.6 km s^{-1} (Hansen et al., 1977). The linear scale is for an assumed distance of 500 pc. The zero of the coordinate scale is $05^h32^m47.58^s \pm 0.02^s$, $-05°24'09''.3 \pm 0''.5$ (1950) (Forster et al., 1978). The spectrum (lower diagram) is that observed at Onsala in February 1977

although declination uncertainties, especially, can sometimes be large (1").

As we discuss later, the fringe visibilities of almost all features are low, that is, the emission is resolved on most baselines (see also Johnston et al., 1977). We are therefore seeing only compact cores or sharp edges in the spatial distribution, rather than the strong H_2O features which dominate single-dish spectra. This point is especially valid for the so-called "shell features" at −5 and +16 km s^{-1} (cf. Genzel and Downes, 1977a; Moran et al., 1977). For this reason, and because many features are blended and have large positional uncer-

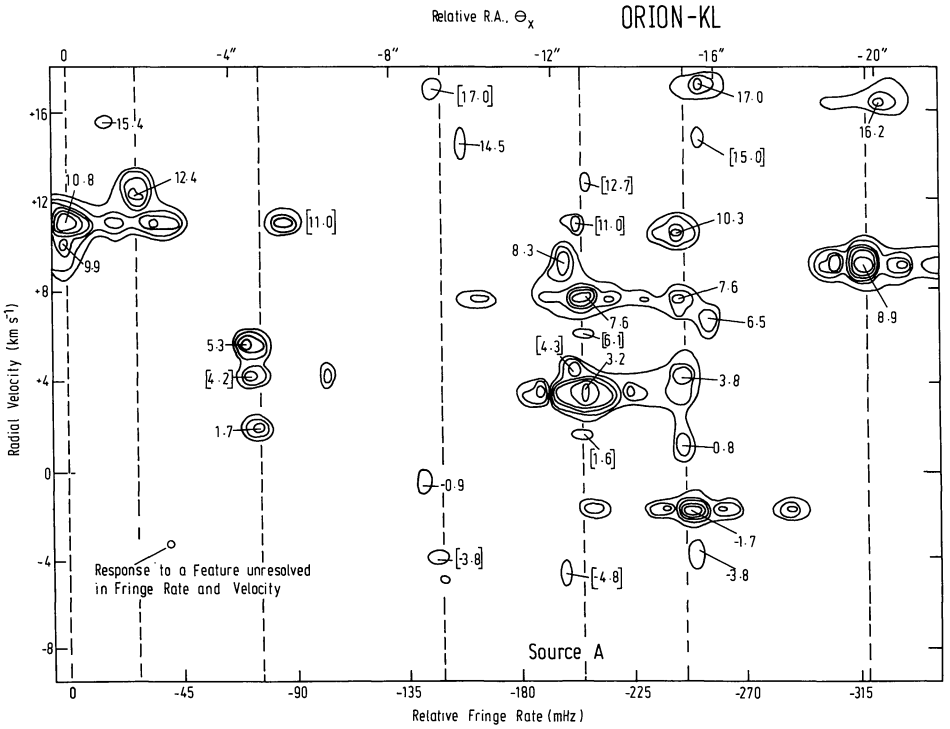

Fig. 5. Diagram of fringe-rate vs. radial velocity (spectral frequency) for sources in Orion-KL. The interferometer baseline was Onsala-Bonn, and the fringe rate information is almost entirely in right ascension. Labels are LSR velocities, in km s^{-1}, as in Figure 4. There are often several features at the same velocity but at different positions. In these cases, the secondary features are indicated in brackets. Vertical lines denote the locations of the "centers of activity" shown in Figs. 4 and 6. For reasons of clarity, we have omitted some weaker sidelobes. Contour units are 1, 5, 10, 15, 25 and 50% of the strongest feature at 10.8 km s^{-1} (6000 Jy)

tainties, we do not think it worthwhile to make a detailed model of the velocity structure in Orion from this map. In general, however, the sources in Orion-KL probably follow the same scheme which we will describe for W 51 M and NGC 7538 S.

The centers of H_2O activity are in or near the KL nebula. The spatial distributions of the H_2O "centers" and the infrared stars are similar; for example, the mean separation between H_2O centers is about the same as that between IR stars. The dominant H_2O, OH and SiO source ("Source A" in Fig. 6) appears to coincide with the compact infrared source IRc4, which has a total luminosity $\geqq 10^4\ L_\odot$ (Rieke et al., 1973). Most of the other H_2O sources do not have infrared counterparts. Source A is either qualitatively different from the other H_2O sources, or else the infrared measurements have missed the weaker sources.

Source A is somewhat unique in that its "shell features" at -5 and $+16$ km s^{-1} agree in velocity with SiO and OH maser lines, and are resolved even on short baselines. However, it is similar to the other H_2O centers in overall size (10^{16} cm), velocity range (10–30 km s^{-1}) and H_2O luminosity (10^{-5}–$10^{-4}\ L_\odot$). It seems more likely that there is only a slight quantitative difference between Source A and the other H_2O centers. The absence of infrared emission at the position of some of the H_2O centers is presumably a matter of sensitivity. The stars in these other centers may be of smaller mass than Source A, or of lower surface temperature or subject to greater extinction, even at 21 μ. The last explanation is supported by two examples: the core of the Sgr B2 molecular cloud is optically thick even for wavelengths > 50 μ (Gatley et al., 1978), and the source C1 in K3–50 (the OH and H_2O source ON-3) has several hundred magnitudes of visual extinction (Wynn-Williams et al., 1977a).

If the high velocity features in Figure 6 are fragments of matter blown out by stellar winds (Strelnitskii and Syunyaev, 1972), it is not clear whether each fragment has come from the nearest "center of activity", or from one dominant source, possibly Source A itself. The high velocity H_2O fragments may be related to the outward flow seen in other molecules. The high velocity wings of ^{12}CO in the $J=1\rightarrow0$, $2\rightarrow1$ and $3\rightarrow2$ transitions appear to come from a dense ($n_{H_2} > 5\ 10^5$ cm^{-3}), hot ($T_{kin} > 100$ K) region roughly centered on the Kleinmann-Low nebula. The half-power width of the high velocity region may be $\leqq 30''$ (Scoville, 1977; Zuckerman et al., 1976; Kwan and Scoville, 1976; Wannier and Phillips, 1977; Phillips et al., 1977).

The "line" of *single* H_2O features, which appeared to run northeast-southwest in some earlier observations,

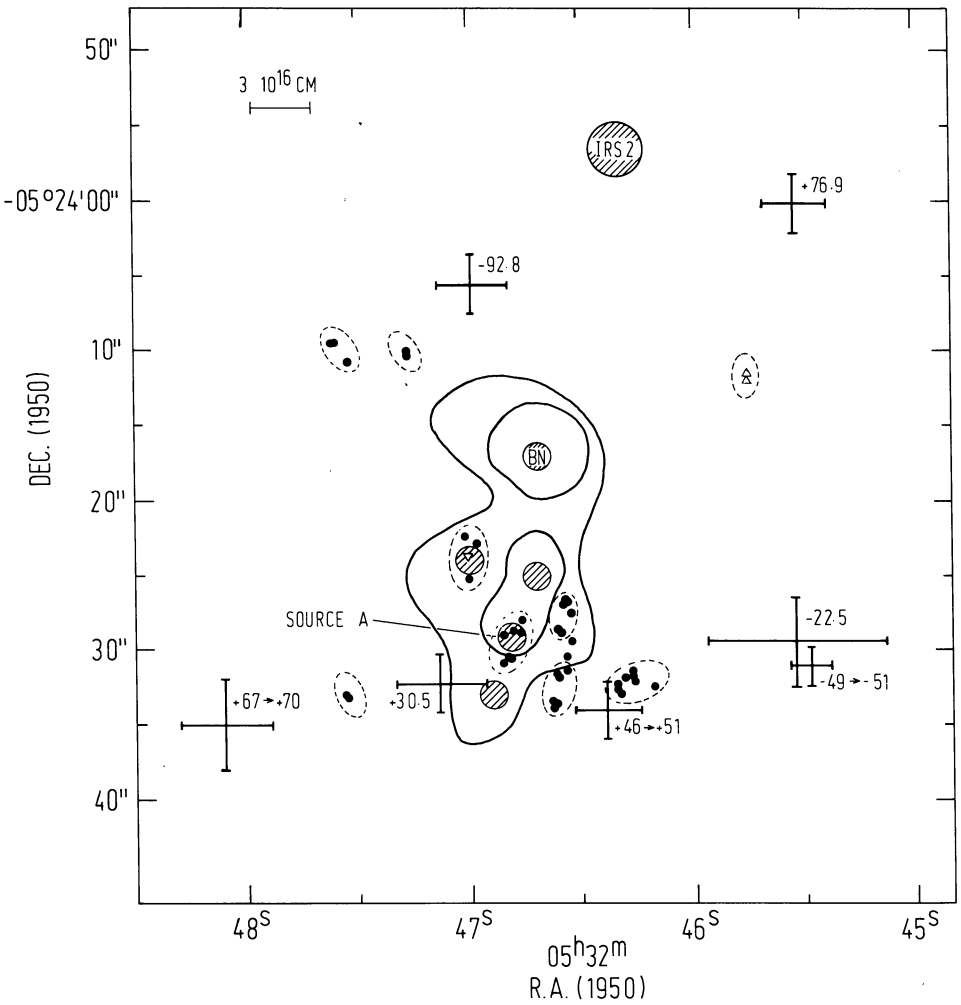

Fig. 6. Positions of H_2O sources in the Kleinmann-Low nebula in Orion. The VLBI positions of the low-velocity H_2O features (Fig. 4) are shown as small circles, superimposed on the contours of 21 μ infrared radiation from the KL nebula (Rieke et al., 1973; Wynn-Williams and Becklin, 1974). The VLBI positions have been calibrated with the Hat Creek position of the feature at +10.8 km s^{-1} (Forster et al., 1978). Dashed lines indicate possible boundaries of "centers of activity" for the low-velocity H_2O emission. Crosses show the positions of weak, high velocity features, measured at Effelsberg in Fall 1976 (Genzel and Downes, 1977a). Labels next to the crosses are LSR velocities in km s^{-1}. Shaded circles indicate compact infrared sources. The linear scale is for an assumed distance of 500 pc. Source A is the dominant H_2O source discussed in the text

disappears in maps with sufficient sensitivity. The whole region, including the KL nebula, the molecular cloud and the cluster of "centers of activity" obviously has a somewhat elongated shape. Attempts to correlate the H_2O with the lower contours of the 5 GHz continuum map by Martin and Gull (1976) should be regarded with caution, however.

Sgr B2

The present observations are the first VLBI results on Sgr B2 (for recent single-dish work, see Genzel et al., 1976, and references therein). Because the common observing time for Sgr B2 is short for VLBI stations in the northern hemisphere, the relative position measurements are not as accurate as for the other sources in this paper. In spite of this problem, the VLBI data (Table 5) confirm the picture of three main, compact H_2O sources in Sgr B2. We refer to the three main sources as Sgr B2 North, Middle and South. In Sgr B2 N, some of the features are spread over 2″ or 3 10^{17} cm. Sgr B2 N may thus be a cluster of H_2O centers as in W3-IRS5 or Orion KL. Sgr B2 M showed fringes in our experiment, but their intensities were not sufficient for accurate position measurements. Table 5 shows that most of the H_2O features in Sgr B2 S are contained within a zone of 0.2″, which corresponds to 3 10^{16} cm, the typical size of a "center of activity". The luminosity of Sgr B2 S is comparable with that of W 51 M.

W*49* N

Our map of December 1976, made from the NRL-Haystack data, agrees well with the map of Walker et al. (1977), and adds a new center of activity (marked by an

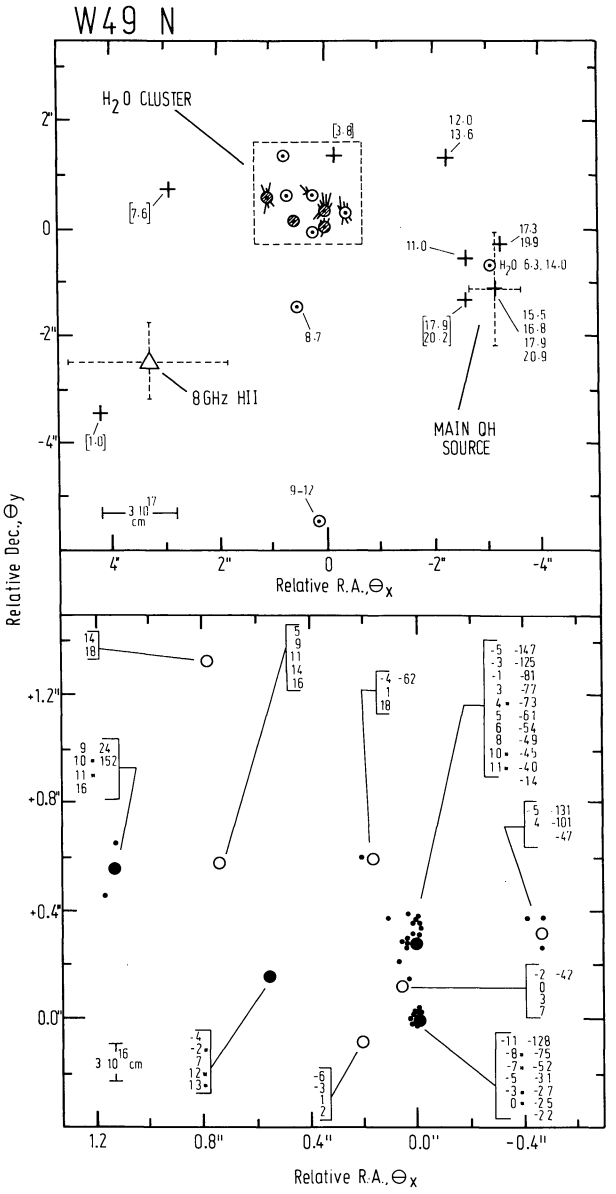

Fig. 7. (upper): Positions of H_2O and OH sources in W 49 N. Dotted circles denote H_2O centers of activity. Shading denotes the strongest "centers". "Centers of activity" which have "high velocity features" are marked by radial dashes. Crosses denote OH masers (Harvey et al., 1974; Mader et al., 1975, 1977). Labels are radial velocities for OH (1667 MHz in bracketts, otherwise 1665 MHz). The dashed cross with triangle gives the positional uncertainty of the nearest compact H II region (Wink et al., 1975). The linear scale is for an assumed distance of 14 kpc.

(Lower): an enlargement of the dashed rectangle in the upper diagram. Only H_2O features are shown. Large circles denote centers of low-velocity H_2O activity. Filled large circles are the strongest centers of activity. Small dots denote high-velocity H_2O features. Labels are H_2O radial velocities (km s^{-1}) contained in each center of activity. Asterisks denote strongest components in the past six years. The diagrams shown here are composites from data obtained in several experiments (Moran et al., 1973; Knowles et al., 1974; Mader et al., 1975, 1977; Walker et al., 1977, and this paper). The high velocity H_2O data are from Walker et al. The zero of the coordinate scale is $19^h07^m49.78^s \pm 0.02^s$, $+09°01'17''.1 \pm 0''.4$ (1950) (Dieter et al., 1978)

Table 5. Relative Intensities and Positions of H_2O Features in Sgr B2 in February 1977

V_{LSR} (km s^{-1})	Average Relative Intensity [a] (per cent)	Relative Position [b] θ_x (R.A.) (milli arc sec)	θ_y (Dec.) (milli arc sec)
Sgr B2 North:			
(Relative to 41.5 km s^{-1}):			
40.6	20	- 90 ± 80	- 74 ± 80
41.5[c]	30	0	0
-			
(Relative to 62.8 km s^{-1}):			
49.9	12	- 149 ± 70	+ 43 ± 30
50.8	10	+1000 ± 80	-1550 ± 30
52.5	6	-1160 ± 150	+ 890 ± 60
56.1	10	+1950 ± 400	+ 660 ±150
62.8[c]	100	0	0
Sgr B2 South:			
51.5	3	- 190 ± 200	+ 100 ± 30
57.6	4	- 70 ± 200	+ 70 ± 15
61.8	5	- 60 ± 200	+ 79 ± 15
63.9	10	- 110 ± 100	+ 96 ± 10
65.2	6	- 220 ± 80	+ 100 ± 30
66.2	4	- 90 ± 150	+ 81 ± 15
67.3	3	+1030 ± 500	- 940 ± 60
69.8[d]	100	0	0
72.3	17	- 120 ± 150	+ 78 ± 10
73.0	8	- 250 ± 50	+ 91 ± 3

[a] From cross-correlation spectrum; 100 % = 400 Jy (Sgr B2 N); 1000 Jy (Sgr B2 S).

[b] Errors are two standard deviations.

[c] Reference features for Sgr B2 N: (0,0) = $17^h44^m10.03^s \pm 0.03^s$, $-28°21'16.3'' \pm 1''$ (1950). (Forster et al. 1978)

[d] Reference feature for Sgr B2 S: (0,0) = $17^h44^m10.6^s \pm 0.3^s$, $-28°22'39'' \pm 4''$ (1950).

Fringes were detected on Sgr B2 M, but the intensity in Feb. 77 was not sufficient for accurate measurements. The 1950 position of Sgr B2 M is $17^h44^m10.4^s \pm 0.3^s$, $-28°22'00'' \pm 4''$ (Genzel and Downes 1977b).

asterisk in Table 6), slightly to the southeast of the two main centers, plus a single, new feature located about 1″.2 to the northeast of the main groups, at a radial velocity of 18.2 km s^{-1}.

Figure 7 (upper) shows that there are about ten centers of activity in W 49 N, most of which lie in a region of size 3 10^{17} cm. This is the same size as the H_2O clusters in Orion and W 3-IRS 5. The *strongest* centers of activity in W 49 N seem to be more compact, however, than in the latter sources (Walker, 1977). The H_2O cluster is clearly separated from the H II region (Wink et al., 1975) and the main OH source (Harvey et al., 1974; Mader et al., 1975, 1977). Figure 7 (upper) also shows that there are some weaker H_2O and OH features spread out over the whole region. On the plot of fringe rate vs. spectral frequency for W 49 N, we detected weak H_2O features at velocities of +6.3 and +14.0 km s^{-1}, which appear to come from the vicinity of the main OH source.

Figure 7 (lower) is an enlargement of the dashed rectangle in the upper diagram. The radial velocities given for the "low velocity features" are an average

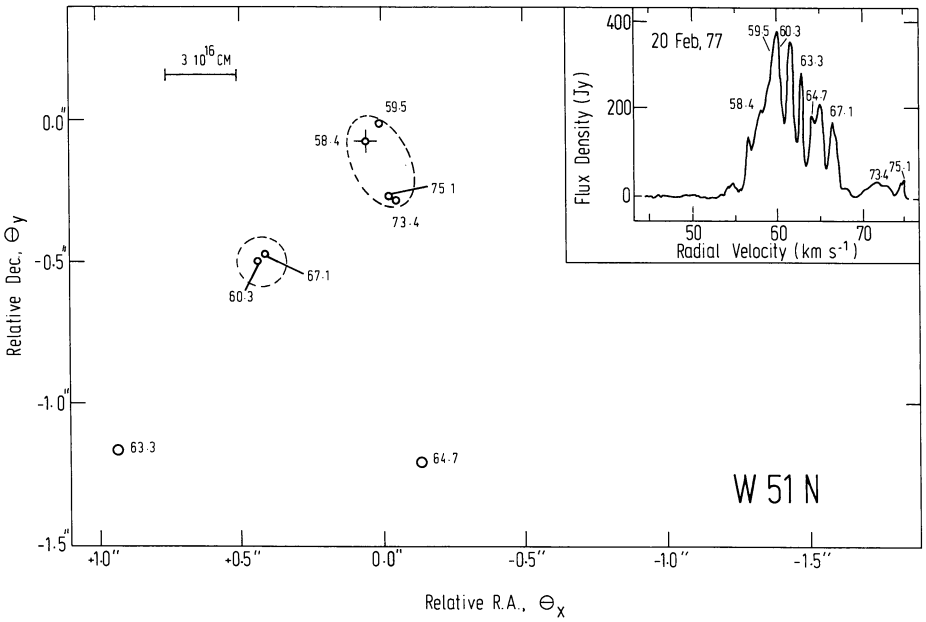

Fig. 8. Positions of the strong, low-velocity H_2O sources in W 51 N, relative to the feature at $+59.5$ km s^{-1}, in February 1977. Labels are LSR velocities (km s^{-1}). Relative positional uncertainties are indicated by circles. Dashed lines indicate possible "centers of activity". The linear scale is for an assumed distance of 8 kpc. The inset shows the single-dish spectrum of W 51 N obtained at Effelsberg in February 1977. The zero of the coordinate scale is $19^h21^m22\overset{s}{.}3 \pm 0\overset{s}{.}2$, $+14°25'19'' \pm 3''$ (1950) (Genzel and Downes, 1977b)

from several experiments in the last six years (Moran et al., 1973; Knowles et al., 1974; Mader et al., 1975, 1977; Walker et al., 1977; and this paper). The mean velocity of the centers of activity increases from ~ -5 km s^{-1} in the southwest to $\sim +12$ km s^{-1} in the northeast, possibly indicating a large-scale gradient. Figure 7 (lower) shows that several of the "centers" are surrounded by swarms of high-velocity features. These high velocity data are taken from Walker et al. (1977).

W *51* N

W 51 N lies 1.5 northwest of the main H_2O source in W 51, and near the compact continuum component labelled G 49.5–0.4(d) on the map by Martin (1972). The H_2O source has an interesting, broad spectrum ranging from -150 to $+150$ km s^{-1}. The strongest emission ($\sim$400 Jy) occurs between velocities of 0 and 70 km s^{-1}. Figure 8 shows the map of radial velocities between 49 and 76 km s^{-1}, obtained from the Onsala-Crimea baseline (Table 7). The features extend over a region of size 1″, with two possible, main concentrations separated by 0″.5. This corresponds to a projected linear separation of 6 10^{16} cm if the source is at a distance of 8 kpc, or 2 10^{16} cm if the H_2O velocity centroid is 35 km s^{-1} and the kinematic distance is 2 kpc. It is not clear whether the results show two or more independent sources or a single, extended source in a later stage of evolution.

W *51 Main and South*

Figure 9 shows the relation of the southern and main H_2O sources in W 51 (Table 8). The H_2O lines at 51.0 and 57.8 km s^{-1} probably come from W*51* S, a source whose spectrum between -10 and $+5$ km s^{-1} was reported by Genzel and Downes (1977b). W 51 S also appears to be associated with 1665 MHz OH emission at 58 km s^{-1} (Mader et al., 1977) and to be near a compact H II region (Scott, 1978).

The emission of the strong H_2O source W 51 M in the velocity interval 49 to 76 km s^{-1} is concentrated to a region of 0″.25 (3 10^{16} cm) indicated by the dashed ellipse in Figure 9. There are also some weaker features spread over a zone of 2 10^{17} cm. Scott (1978) has found a supercompact H II region 2″.2 $\pm$ 0″.8 away from the H_2O source, with the Cambridge 5-km telescope at 15 GHz. On the basis of this positional displacement, we think that the exciting star of the compact H II region does *not* provide the energy for the H_2O source W 51 M.

Figure 10 shows that except for the line at 68.7 km s^{-1}, all of the strong H_2O lines are concentrated to an even smaller region of 60 milli arc sec or 7 10^{15} cm. Two knots of about equal intensity and similar velocity structure, which are separated by only 7.5 10^{14} cm, contain 60% of the total luminosity (see inset in Fig. 10). The map in Figure 10 leads us to the following conclusions.

a) If the weaker, more extended features are regarded as "high velocity features", the 2″ (2 10^{17} cm) extent of

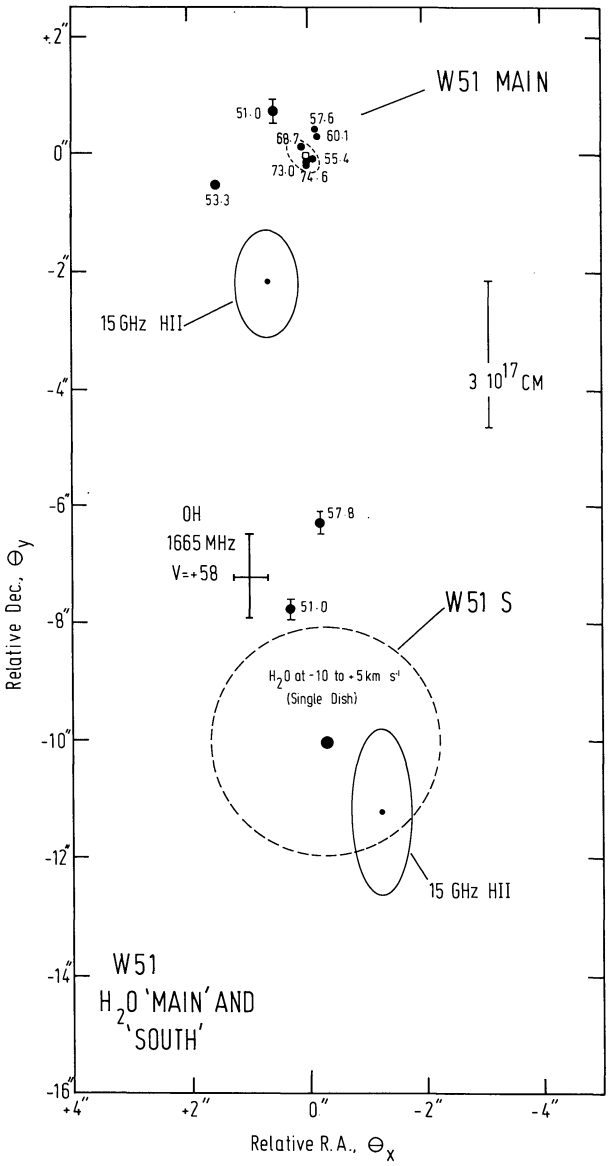

Fig. 9. Positions of maser features in the H_2O sources W 51 Main and W 51 South in February 1977, relative to the feature at 62.5 km s^{-1}. Labels are LSR velocities in km s^{-1}. Small dots are VLBI measurements, and the dashed circle gives the positional uncertainty in the singledish position for features at $V_{LSR} = -10 - +5$ km s^{-1} (Genzel and Downes, 1977b). The small dashed ellipse contains most of the H_2O flux of W 51 M, and is shown in enlargement in Figure 10. The cross is the position of the OH maser at 1665 MHz, with $V_{LSR} = +58$ km s^{-1} (Mader et al., 1977). The linear scale is for an assumed distance of 8 kpc. The zero of the coordinate scale is $19^h21^m26\overset{s}{.}20 \pm 0\overset{s}{.}02$, $+14°24'43\overset{''}{.}6 \pm 0\overset{''}{.}4$ (1950) (Forster et al., 1978). The solid ellipses give the positional uncertainties for continuum sources measured with the Cambridge 5-km telescope at 15 GHz (Scott, 1978)

Table 6. Relative Intensities and Positions of H_2O Features in W49 N in December 1976

V_{LSR} (km s^{-1})	Average Relative Intensity [a] (per cent)	Relative Position [b] θ_x (R.A.) (milli arc sec)	θ_y (Dec.) (milli arc sec)
- 8.3	0.1	0 ± 80	+ 20 ± 200
- 7.9	0.2	+ 52 ± 80	+ 120 ± 200
- 6.2*	0.6	+ 200 ± 30	- 82 ± 80
- 4.7	4	+ 15 ± 20	+ 290 ± 60
- 4.1	4	+ 200 ± 40	+ 626 ± 150
- 2.6	6	+ 559 ± 20	+ 155 ± 40
- 0.3 [c]	14	0	0
1.4	2	+ 181 ± 40	+ 555 ± 100
2.7	8	+ 40 ± 60	+ 590 ± 200
4.0	1.5	- 100 ±100	+ 250 ± 200
5.2	2	- 5 ± 40	+ 450 ± 100
6.3	2	+ 10 ± 30	+ 245 ± 80
7.1	3	+ 25 ± 20	+ 80 ± 60
8.2	5	+ 11 ± 6	+ 290 ± 20
9.4	2	+1123 ±180	+ 391 ± 500
10.9	100	- 5 ± 6	+ 291 ± 20
11.8	7	+1112 ± 20	+ 561 ± 60
16.0	3	+ 733 ± 40	+ 589 ± 100
17.5	1.5	+ 126 ± 20	+ 570 ± 60
18.2	0.7	+ 760 ± 80	+1340 ± 200

a) From cross-correlation spectrum; 100 % ~90 000 Jy.

b) From Haystack-NRL baseline; errors are two standard deviations.

c) Reference feature; (0,0) = $19^h07^m49.78^s \pm 0.02^s$, $09°01'17.1'' \pm 0.4''$ (1950), (Dieter et al. 1978).

Table 7. Relative Intensities and Positions of H_2O features in W51N in February 1977

V_{LSR} (km s^{-1})	Average Relative Intensity [a] (per cent)	Relative Position [b] θ_x (R.A.) (milli arc sec)	θ_y (Dec.) (milli arc sec)
58.4	20	+ 65 ± 40	- 88 ± 40
59.5 [c]	40	0	0
60.3	60	+442 ± 10	- 490 ± 10
63.3	100	+939 ± 10	-1162 ± 10
64.7	20	-135 ± 8	-1212 ± 8
67.1	25	+427 ± 8	- 470 ± 8
73.4	10	- 44 ± 40	- 274 ± 30
75.1	10	- 38 ± 10	- 270 ± 10

a) From cross-correlation spectrum; 100 % = 380 Jy.

b) Onsala-Crimea baseline; errors are two standard deviations.

c) Reference feature; (0,0) = $19^h21^m22.3^s \pm 0.2^s$, $14°25'19'' \pm 3''$ (1950) (Genzel and Downes, 1977b)

the region in which they are found is comparable with that of the high velocity features in Orion, and larger than that in W 49.

b) The strong "low velocity emission" of W 51 M is concentrated in a "belt" of length 3 10^{16} cm and width 5 10^{15} cm, running northeast-southwest. It is likely that this source represents only *one* object. The two central knots *both* have emission at ~63 and ~69 km s^{-1}, at about equal intensities. More detailed observations of this source show that the two knots have an almost identical velocity structure (Walker, 1977). There obviously has to be a high degree of symmetry in any model

Table 8. Relative Intensities and Positions [b] of H_2O Features in W51 M and W51 S

	December 1976			February 1977		
		Relative Position			Relative Position	
V_{LSR} (km s^{-1})	Average Relative Intensity [a] (per cent)	θ_x (R.A.) (milli arc sec)	θ_y (Dec.) (milli arc sec)	Average Relative Intensity [a] (per cent)	θ_x (R.A.) (milli arc sec)	θ_y (Dec.) (milli arc sec)
50.4		—	—	0.1	- 507 ± 400	1162 ± 200
51.0 [c]	5	+292 ± 40	-7728 ± 40	1	557 ± 15	770 ± 200
53.3		—	—	1	1530 ± 40	- 515 ± 20
53.8	70	- 14.3 ± 8	- 5.7 ± 10		—	—
54.6		—	—	26	- 25.0 ± 1.5	- 13.6 ± 0.8
55.4		—	—	5	- 62.7 ± 8	- 97.7 ± 4
55.9	100	- 12.9 ± 15	1.4 ± 15		—	—
56.5		—	—	28	- 35.0 ± 2	- 46.5 ± 1
57.0	7	-172 ± 100	307 ± 150	8	- 18.2 ± 8	- 10.3 ± 4
57.6		—	—	5	- 206.2 ± 6	369.3 ± 2
57.8 [d]	5	-233 ± 1500	-6429 ± 1500	5	- 225 ± 6	-6309 ± 200
59.7		—	—	5	+ 7.5 ± 2	7.7 ± 1.5
60.1	7	-159.5 ± 100	273 ± 150	13	- 212.0 ± 15	263 ± 80
60.9		—	—	3	0.8 ± 6	8.0 ± 3
62.5 [e]	30	0	0	100	0	0
63.6	60	- 7.4 ± 7	10.8 ± 8	17	- 3.1 ± 2	- 5.8 ± 1
64.3	10	4.6 ± 20	- 15.7 ± 25	3	+ 6.0 ± 4	8.5 ± 3
65.4	20	- 1.1 ± 15	- 1.0 ± 20	10	- 5.0 ± 1.5	- 2.2 ± 0.6
65.6				10	- 1.7 ± 1.5	- 2.6 ± 0.6
67.5	30	- 4.8 ± 5	2.2 ± 8	60	- 2.4 ± 1	- 5.0 ± 0.6
68.7		—	—	40	17.8 ± 2	109.0 ± 0.8
69.6	40	- 6.7 ± 5	10.2 ± 8		—	—
70.0	30	- 21.1 ± 10	41.6 ± 15		—	—
70.5	30	- 5.4 ± 10	- 1.2 ± 10	27	0.6 ± 2	2.4 ± 2
71.1		—	—	10	- 1.3 ± 2	- 0.8 ± 2
72.1	10	7.8 ± 15	6.1 ± 15	5	0.3 ± 0.8	- 0.2 ± 0.4
73.0		—	—	1	- 46.0 ± 10	- 138 ± 6
74.6		—	—	1	- 47.5 ± 6	- 141.3 ± 4
75.2		—	—	5	- 7.9 ± 10	- 12.3 ± 8
75.3		—	—	4	0.6 ± 3	- 27.5 ± 2
75.6		—	—	1	- 9.6 ± 20	- 60.4 ± 20

[a] From cross-correlation spectrum; 100 % = 1400 Jy in Dec. 76; 1150 Jy in Feb. 77.

[b] Errors are two standard deviations.

[c] Emission at 51.0 km s^{-1} was stronger from W51 S in Dec. 76, and from W51 M in Feb. 77.

[d] W51 S.

[e] Reference feature; (0,0) = $19^h21^m26.20^s \pm 0.02^s$, $14^o24'43.6'' \pm 0.4''$ (1950)(Forster et al. 1978).

which accounts for the H_2O emission, in order to produce such a double velocity, double knot structure.

c) The single-dish spectrum of W 51 M averaged over roughly two years show three main, stable, groups of lines, even if the symmetry was not always as striking as in February 1977 (Fig. 10, inset; see also the data of Little et al., 1977).

In the following section, we present two qualitative models for the kinematics of W 51 M. The general picture of an expanding dust shell, bounded on the inner side by a dust front and on the outer side by a shock front, has been adopted from Davidson and Harwit (1967), de Jong (1973), Kahn (1974), Yorke and Krügel (1977), and Cochran and Ostriker (1977). The first model is of an expanding and rotating disk. The second model is an expanding spherical shell which sporadically ejects faster-moving features.

Figure 11a shows the first model. The ellipsoidal dust shell or disk, with a radius of 1.5 10^{16} cm and a thickness of 3 10^{15} cm, is observed almost edge-on. The H_2O features at $\sim$55 and $\sim$69 km s^{-1} are at the front and back of the disk, and the central star has a radial velocity of 63 km s^{-1}. The line at 68.7 km s^{-1} comes from the edge of the disk; its velocity suggests that the disk may be rotating at about 6 km s^{-1}. The star would then have a mass of 20–40 $M_\odot$. The features at a relative velocity of $\sim$0 km s^{-1} originate outside a shock front which expands at a velocity of 6 to 8 km s^{-1} into the surrounding medium.

High velocity features could be envisaged as being driven out along the poles of the disk. The model in Figure 11a requires a large stellar mass to account for rotational velocities of 6 to 8 km s^{-1}. A model with expansion only (Fig. 11b) means that all lines *other* than

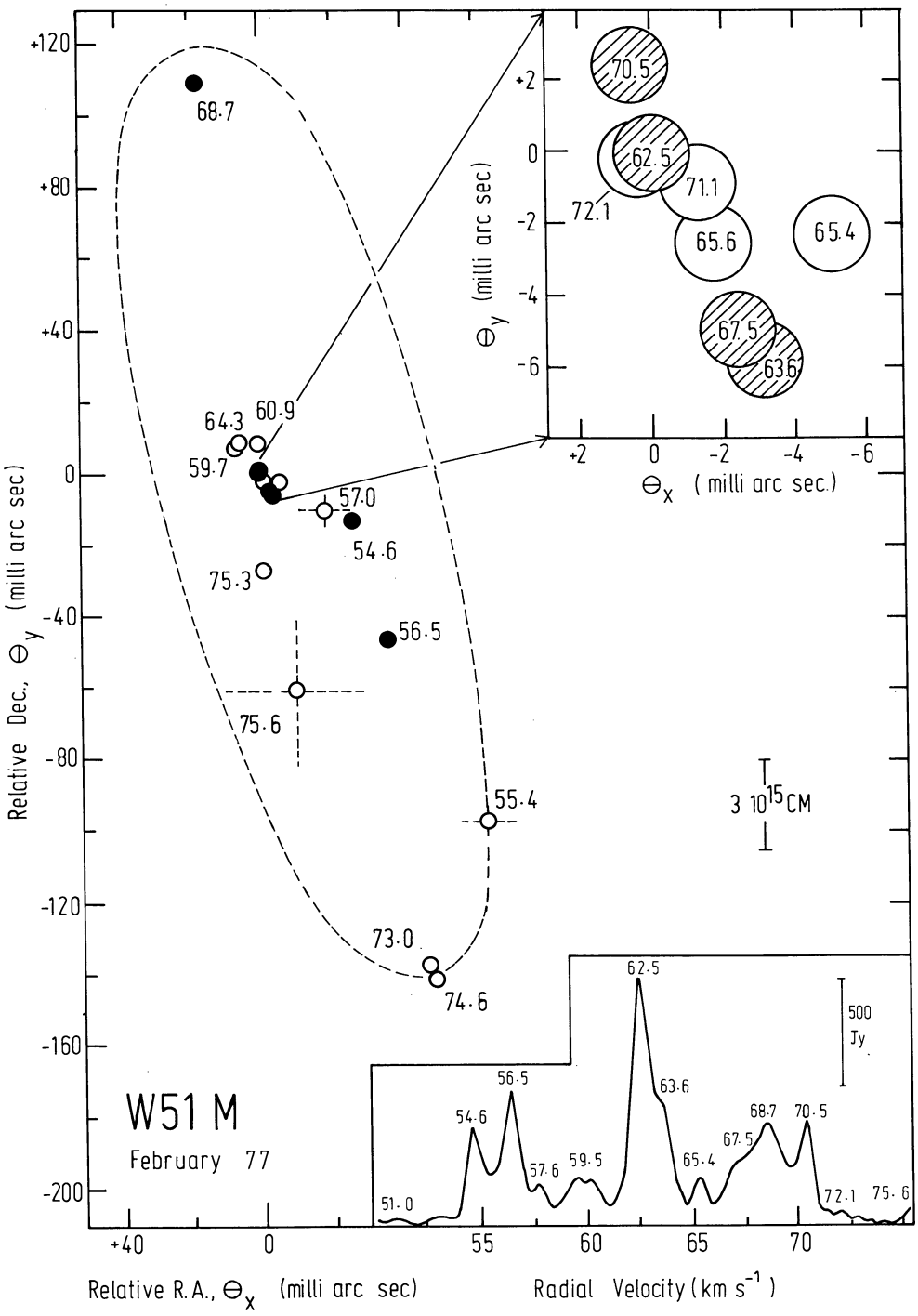

Fig. 10. Positions of strong, low-velocity H_2O emission in W 51 Main in February 1977. The positions are relative to the feature at 62.5 km s^{-1}. The figure is an enlargement of the small ellipse shown in Figure 9. The inset to the right is in turn an enlargement of the intense maser group near the center of *this* figure. The relative positional uncertainties ($\sim 2\sigma$ for the main figure, 1σ for the inset) are given by shaded circles for strong (>300 Jy) features, and unshaded circles for weaker features. Error bars larger than the general mean are indicated by dashed crosses. Labels are LSR velocities in km s^{-1}. The linear scale is for an assumed distance of 8 kpc. The central knots discussed in the text are the main shaded groups in the inset. The inset at the bottom right shows the single-dish spectrum of the low-velocity emission, obtained at Effelsberg in February 1977. The dashed ellipse shows the region interpreted in the text as being a circumstellar disk. The coordinate zero is the same as in Figure 9

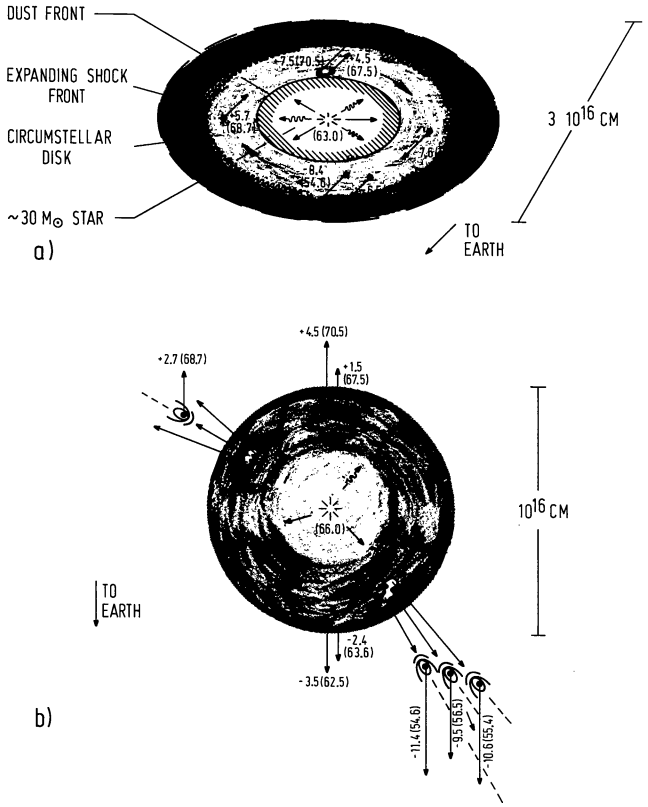

Fig. 11. Kinematic models of W 51 M. The H_2O emission is presumed to arise in a dense, expanding disk or shell around a massive star. The labels give the line-of-sight velocities relative to the star; observed LSR velocities are in parentheses (cf. Fig. 10).

Model a): an expanding and rotating disk observed nearly edge-on. The radial velocity of the star is 63 km s^{-1}, the expansion and rotation velocities are both ~7 km s^{-1}. The H_2O features at ~0 km s^{-1} could come from either the front or back of the disk, slightly outside the shock front. High velocity features could be blown out at the poles of such a disk.

Model b): an expanding shell, viewed perpendicular to the line of sight to the earth. The star, with V_{LSR} ~66 km s^{-1}, has directional flares from time to time, which drive higher-velocity material through holes or tunnels in an otherwise stable shell. The shell expands at a velocity of 3 km s^{-1}

those emitted in the inner 0".03 are "high velocity features". The central star may flare from time to time, and burn "holes" or "tunnels" in the circumstellar shell. The alignment of H_2O features in W 51 M and W 3(OH) might then indicate the direction of temporary, high-density streams. The entire shell could nevertheless be stable over long periods of time.

NGC *7538*-IRS *1*

NGC 7538-IRS 1 appears to coincide, within 0".5, with a strong infrared source, IRS 1, and a super-compact H II region (Harris and Scott, 1976; Wynn-Williams et al., 1974; Willner, 1976; Genzel and Downes, 1977b). Fringes were obtained on the lines at −60.7 and −57.2 km s^{-1}, which were separated by 0".28 or 1.5 10^{16} cm (Table 9).

Table 9. Relative Intensities and Positions of H_2O Features in NGC7538 in February 1977

V_{LSR}	Average Relative Intensity[a]	Relative Position[b] θ_x (R.A.)	θ_y (Dec.)
(km s^{-1})	(per cent)	(milli arc sec)	
NGC7538 - IRS 1:			
-57.2	10	+275.8 ± 0.6	+12.5 ± 0.2
-60.7[c]	100	0	0
NGC7538 S:			
-45.0[c]	100	0	0
-48.2	10	-142 ± 15	+ 75 ± 20
-53.5	80	+ 64 ± 2	-180 ± 2
-54.2	60	-144 ± 1	-125 ± 1.5
-54.8	20	+ 78 ± 4	-157 ± 4
-56.3	20	- 87 ± 6	-304 ± 7
-61.3	100	- 40 ± 3	+113 ± 4

a) From cross-correlation spectrum; 100 % = 600 Jy for NGC7538-IRS1 and 150 Jy for NGC7538S.

b) Errors are two standard deviations.

c) 1950 positions for reference features:

(0,0) = { $23^h11^m36.47^s \pm 0.05^s$; $+61°11'49.4'' \pm 0.5''$ } NGC7538-IRS1

(0,0) = { $23^h11^m36.14^s \pm 0.05^s$; $+61°10'29.7'' \pm 0.5''$ } NGC7538S

from data of Förster et al. (1978).

NGC *7538* S

NGC 7538 S lies 1'.5 south of IRS 1, and has OH emission at roughly the same velocities as the H_2O. Wynn-Williams et al. (private communication) have found far infrared and millimeter radiation from this source, but no near infrared emission. There is also no radio emission, to a limit of 5 mJy at 5 GHz (Israel, 1977). If there is an optically thick H II region in NGC 7538 S, it must have a size smaller than 0".15. These facts suggest that NGC 7538 S is cooler or more obscured in the near infrared than IRS 1, which *is* associated with a compact H II region, of diameter 1".

As with IRS 1, the small spatial extent of the H_2O source (Fig. 12) of 0".4 (2 10^{16} cm) indicates that NGC 7538 S is a single object, similar in many respects to W 51 M. Figure 12 includes the VLBI data of Moran et al. (1978) from January 1974, which agree nicely with the new results. The H_2O spectrum appears to be an asymmetric "triple", with some weak emission between the main components. Figure 12 also shows a model of NGC 7538 S as an expanding disk inclined to the line of sight.

Sizes of Individual H_2O Features

We now discuss the investigation of fringe visibilities of three sources, W 3(OH), Orion-KL and W 51 M. The

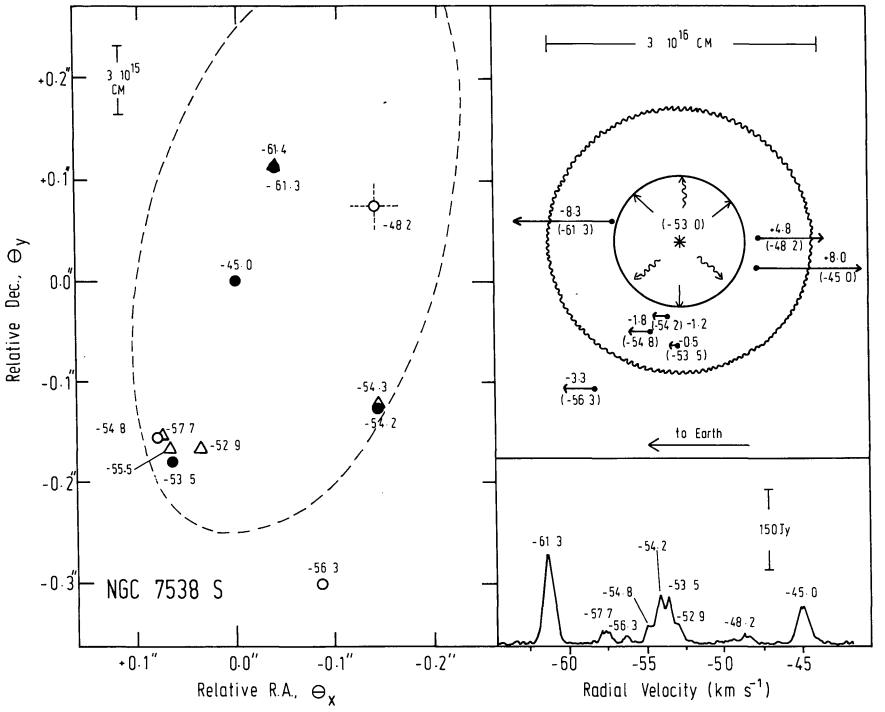

Fig. 12. *(left)*: Relative positions of H_2O masers in NGC 7538 S, in February 1977. The positions are relative to the feature at -45.0 km s^{-1} and the zero of the coordinate scale is $23^h11^m36^s.14 \pm 0^s.05$, $+61°10'29''.7 \pm 0''.5$ (1950), from Forster et al. (1978). Average positional uncertainties are indicated by shaded circles for strong (>100 Jy) features and by open circles for weaker features. Triangles are positions measured in a VLBI experiment of January 1974 (Moran et al., 1978).

The linear scale is for an assumed distance of 3.5 kpc. The lower inset shows the single dish spectrum obtained at Effelsberg in February 1977.

(Upper right): Model of NGC 7538 S in terms of a disk inclined at an angle of ~30° to the line of sight. Labels give velocities (km s^{-1}) relative to $V_{LSR} = -53.0$ km s^{-1}, the assumed velocity of the central star. Values in parentheses are the observed LSR velocities. The disk is assumed to be expanding at 9 km s^{-1}. The length of the arrows are proportional to the *relative* velocity components in the direction of the earth

conclusions probably apply to the other sources in this survey as well. A characteristic of the VLB network used here is that the best linear resolution in W 51 is the same as the poorest linear resolution in Orion, namely $4\ 10^{13}$ cm. Overall, the experiment is sensitive from $3\ 10^{12}$ cm to $6\ 10^{14}$ cm in spatial structure.

In W3(OH) and W 51 M, the visibilities of the strongest features are high, that is, between 0.4 and 1.0, on all baselines, indicating that the masers are smaller than $4\ 10^{13}$ cm (~3 A.U.) in apparent size. In W 51 M, there is some evidence that minor features (>200 Jy in the single-dish spectra) are resolved, even on the shortest baseline.

Most of the Orion features are also unresolved on the shortest baseline, which means that the upper limit to their size is, again, $4\ 10^{13}$ cm. Only the prominent shell features at -5 and $+16$ km s^{-1} in Source A, and the strong feature at $+5.3$ km s^{-1}, in the northeastern part of the Orion map, have low visibilities on the Onsala-Effelsberg baseline. *All* features in Orion are completely resolved on the Haystack-Effelsberg baseline, which shows that these H_2O masers are not much smaller than 10^{13} cm (~1 A.U.). From this size, and the typical line flux density of 10^3 to 10^4 Jy, the line brightness temperature is $\sim 10^{12}$ to $\sim 10^{13}$ K.

The visibility of some features in Orion and W3(OH), and to a lesser extent, in W 51 M, changes systematically with interferometer hour angle. The typical time scales of the variation are hours, which may correspond to structure on an angular scale of 5–10 milli arc sec, or 10^{14}–10^{15} cm. This structure resembles the "double knots" in W 51 M. Some lines in the single-dish spectra are not visible in the cross-correlation spectra. They may be much larger clouds, like the "shell features" of Source A in Orion.

Models of H_2O Sources

We summarize here basic observational facts which must be incorporated in models of H_2O sources.

1. Spatial Structure

a) Nearly all of the individual "centers of activity" described in this paper show *low velocity* H_2O *features* distributed over $\sim 10^{16}$ cm. The map of W 51 M provides evidence for disk structure in one of these centers.

b) *Individual masers* have an apparent diameter of 10^{13}–10^{14} cm. In Orion-KL, W 3-IRS 5 and W3(OH), a given radial velocity sometimes seems to come from two different emission knots separated by 10^{14}–10^{15} cm. Maps of W 51 M and CRL 2591 (Walker, 1977) show that two spatially distinct knots can even have many velocity components in common. This phenomenon has been verified in independent experiments, and on independent baselines, and appears to be an important property of the masers.

c) The observations of W 49 N (Walker et al., 1977) and possibly W 51 M (this paper) suggest that some, but not all, centers of activity are surrounded by swarms of *high velocity features* over a spatial extent of $5\ 10^{16}$ –$4\ 10^{17}$ cm. If the weaker lines in W3(OH) are also to be interpreted as "high velocity fragments", they would indicate that such fragments are found in a preferential direction from the "center of activity".

d) Individual centers of activity often appear in *clusters*, of overall size 3 10^{17} cm, with two to ten members, and an average projected separation of 5 10^{16} cm between them (e.g., W 3-IRS 5, W 75 S, Orion-KL, W 49 N). In W 3-IRS 5 and Orion, this also seems to be the typical separation between compact IR sources.

2. Relation to Other Objects

a) Where infrared observations of high resolution and sensitivity are available (e.g. Orion-KL, W 3-IRS 5, NGC 7538, CRL 2591, some Sharpless H II regions), there are infrared sources in the vicinity ($\leqq 10^{17}$ cm) of the H_2O masers. A detailed coincidence, however, between centers of H_2O activity and compact infrared sources (which are not H II regions) exists so far only for IRc 4 (H_2O Source A) and IRc 2, both in Orion-KL, and for CRL 2591 (Wynn-Williams et al., 1977b; Walker, 1977).

b) The strong H_2O masers are near ($\leqq 3\ 10^{18}$ cm) "compact" H II regions but not coincident with them (Lo et al., 1975; Cato et al., 1976; Baudry et al., 1976; Forster et al., 1978; Genzel and Downes, 1977b). The exciting stars of the H II regions, therefore, do not provide the energy for the H_2O masers, except possibly for the stars in new class of "supercompact" H II regions, like NGC 7538-IRS 1 and ON-1.

c) With observations of high sensitivity, one often finds OH maser emission at the same position and radial velocity as H_2O emission (e.g. W 51 S, Orion-KL, NGC 7538, W 49 N?), although the *strongest* OH and H_2O sources in a region may not coincide (Mader et al., 1975, 1977).

d) The lifetime of the H_2O-emitting phase appears from source statistics to be on the order of $\sim 2\ 10^4$ yr, while the time required to form a massive star is 10^5–10^6 yr (see, e.g., Yorke and Krügel, 1977). If the former value is roughly correct, only $\leqq 10\%$ of the newly-formed stars in a region will be H_2O emitters at any given time. If so, the examples of Orion-KL, W 3-IRS 5 and W 49 N, which all have a multiplicity of centers of H_2O activity, suggest then that star formation must have started at about the same time in regions of 3 10^{17} cm in diameter (cf. Elmegreen and Lada, 1977).

3. Kinematics

a) The VLBI and single dish observations of W 51 M, Orion-KL, W 49 N and W3(OH) show that despite the large variability of individual lines, the velocities of the main, low-velocity emission groups remain constant to within ± 0.5 km s^{-1} (Sullivan, 1973; Little et al., 1977).

b) The coarse symmetry in the low velocity emission and the maps of W 51 M and NGC 7538 S, indicate that the sources are either expanding or contracting, with some rotation. The most likely interpretation is expansion. The velocities of ~ 10 km s^{-1} at radii of 10^{16} cm, the high temperatures and densities required to excite the H_2O at these radii, and the existence of high-velocity features at *greater radii from the central star* than the low velocity emission, all suggest that matter is flowing away from the stars. That is, the objects are probably *not* protostars, but stars which have already formed.

We now briefly describe two complimentary aspects of shell models for the kinematics and observed structure of the centers of activity.

i) The "Maximum Maser Gain Model"

Assume that the H_2O is everywhere inverted by the same amount, and that the circumstellar material is homogeneous, and arranged in shells or disks. The positions where an observer will see the strongest maser gain will then be determined by the type of motion (expansion, contraction or rotation), the velocity gradients in the shell, the shell thickness, etc. Figure 13 gives a qualitative idea of the location of the observed "hot spots" and the resulting H_2O spectra for different types of motion in the shell (cf. Van Blerkom and Auer, 1976; Olnon, 1977). Here we presume for simplicity that H_2O masers are partially saturated, so that some non-linear amplification causes only those spots to be observed which have the most favorable gain paths. For example, in W 51 M, the VLB results might be described by a decellerated expansion ($V \propto r^{\alpha}$, where V = velocity, r = radius and $\alpha < 0$), with some rotation. "High velocity features" would have to come from temporary holes in the shells ("tunnel model") or else be blown out at the poles of a disk.

The greatest difficulty with this "homogeneous" picture is the apparent variety of velocity distributions observed in VLB maps. The conditions in the shells would therefore have to vary appreciably from source to source.

ii) The "Planetary" Model

Again, we assume that the star is surrounded by a shell or disk. The location of maser emission is determined not by geometrical effects, however, but simply by the positions of dense blobs of matter. This picture easily explains high velocity features, since only a few dense fragments are required. However, it is hard to account for the spectral symmetry and a long duration of the H_2O emitting phase. If the H_2O lines come from a few of the denser clumps in the shell, then there should not be too much symmetry in the observed spectra. Such clumps cannot be gravitationally bound, and would disperse in $\sim 10^3$ years. Furthermore, with only a few condensations around a star, the obscuration might not be as great as in a shell model, and one might expect to

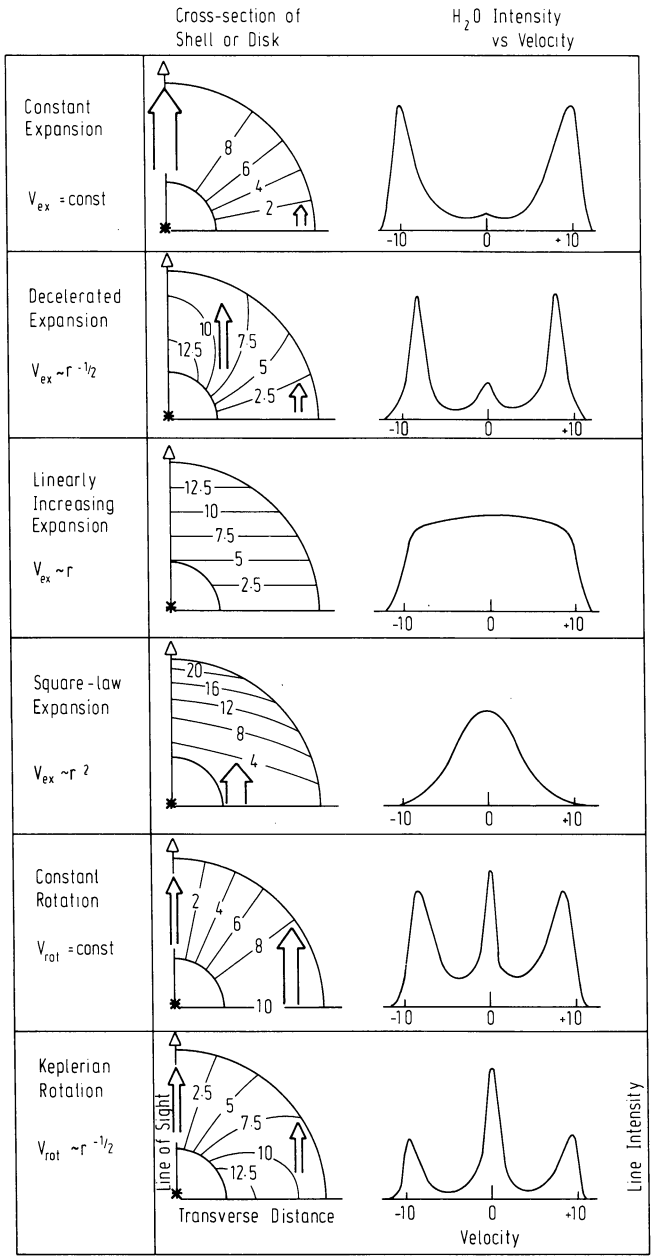

Fig. 13. Qualitative diagram of the expected maser emission from circumstellar shells or disks with various velocity laws. The medium is assumed to be homogeneous with uniform H_2O inversion. The left diagrams show contours of constant velocity as seen by an observer, for one quadrant of the shell. 10 units = the velocity of expansion, contraction or rotation relative to the central star. The arrows are the rays of maximum maser gain as seen from the earth. The diagrams at the right are the expected spectra for the *entire* shell. The second diagram from the top for example, shows that in a decellerated expansion (or free-fall contraction), the spectrum is "triple", and the strongest features will be displaced from the line of sight to the star

see more radio, infrared and optical radiation at the positions of the H_2O sources than is the case.

In reality, these two viewpoints probably must be combined: the motions of a shell or disk determine the general properties of the spectra, averaged over several years. The inhomogeneities govern the positions and velocities of individual spectral features at any given time.

The Infrared Problem

A hot dust shell of temperature 300 K, diameter 10^{16} cm, thickness 10^{14}–10^{15} cm and H_2 density 10^6–10^9 cm^{-3}, has a large optical depth at 10–20 μ and should be a strong infrared source. Many centers of H_2O activity, however, are apparently not detectable IR sources. The upper limit of ~25 Jy on 20 μ radiation from the position of W 51 M for example, (Wynn-Williams et al., 1974) requires an extinction $\tau_{20\mu}=1$ in front of a dust shell with the above parameters. For a mixture of ice, graphite and silicate grains, $\tau_{dust} \approx 5\,10^{-23}$ $n_{H_2}\ell$ at 10–20 μ, where ℓ is the thickness of the cloud in cm (Forster et al., 1978). A cold cloud of radius 10^{17} cm and density 10^6 cm^{-3} would therefore have a large enough optical depth even at 20 μ to reduce the radiation from a 300 K circumstellar dust shell to below the published levels of detection.

An Alternative Explanation

In several well-investigated cases, an H_2O source is near ($<3\,10^{17}$ cm), but not coincident with, a very compact H II region (Forster et al., 1978). As opposed to a "shell" picture, there is therefore a fundamentally different explanation in which the H_2O masers are in small ($<1\ M_\odot$) fragments farther than 10^{17} cm away from the exciting star of the compact H II region, *without* an internal stellar heat source of their own. The shock and ionization fronts of the H II region are assumed to pass through these isolated cloud fragments and collisionally excite the H_2O masers. In this picture, the H_2O masers would appear in an irregular fashion, in a much later evolutionary stage than in the "shell" model.

Although such a model would easily explain why many centers of H_2O activity have not yet been detected in the infrared, it poses some serious problems of its own:

i) In all of the cases investigated by Forster et al., there is only *one* strong center of H_2O activity in the immediate vicinity of the compact H II regions. If the shock fronts from these compact H II regions were simply hitting isolated fragments, one would expect to see several H_2O masers, roughly situated in a ring around the H II regions.

ii) If the plasma in an H II region of density $N_e \sim 10^6$ cm^{-3}, expanding at 10 km s^{-1}, were able to give *all* of its kinetic and thermal energy to a dense cloud of diameter 10^{15} cm, the power transferred would be only 10^{30} erg s^{-1}. The luminosity of the H_2O maser lines in W 51 M, however, is 10^{31} erg s^{-1}. Furthermore, in this sort of collisional pumping, there are at least ten infrared line photons emitted for each photon at 22 GHz

(Goldreich and Kwan, 1974; Shmeld et al., 1976), so that the actual power required to excite the H_2O maser in W 51 M is at least $10^{34\pm2}$ erg s^{-1}. Hence, the kinetic and thermal energy of a shock front from an expanding H II region *cannot* account for the energy continuously radiated by the strong H_2O masers over many years.

iii) For cloudlets located outside of a compact H II region, at distances $>10^{17}$ cm from the exciting star, the radiation from, say, an O 5 star with $3\,10^5\,L_\odot$, is too diluted to heat the dust in the cloudlets to >100 K, even if the cloudlet is optically thick in the near infrared, or to pump the masers by direct radiation (Strelnitskii, 1974).

For the reasons given here, together with the appearance of the VLBI maps, the low and high-velocity emission, and the coarse "symmetry" in the H_2O spectra, we conclude that each center of H_2O activity must have its own source of energy, namely, a massive star.

Acknowledgements. We wish to thank S. Beck, I. Pauliny-Toth, B. F. Burke, L. Bååth, I. Strepka, G. Rydbeck, J. Elldér and E. Kollberg for assistance during the observations, J. Burch for help in the processing, V. A. Kotelnikov, R. Z. Sagdeyev, A. B. Severny, I. S. Shklovsky, V. S. Strelnitskii and P. G. Mezger for their support and for useful discussions. We are especially grateful to the telescope operators and the technicians for their assistance at the different VLBI stations. We thank P. F. Scott, R. Norris, G. L. Mader, J. R. Forster, A. Baudry, W. J. Welch and M. C. H. Wright for providing data prior to publication. The U. S. National Radio Astronomy Observatory is operated by Associated Universities, Inc., under contract with the U. S. National Science Foundation. Onsala Space Observatory is operated by the Research Laboratory of Electronics, Chalmers University of Technology, Gothenburg, with financial support from the Swedish National Science Research Council and the Swedish Board for Technical Development.

References

Baudry, A., Forster, J. R., Welch, W. J., Wright, M. C. H.: 1976, *Bull. Am. Astron. Soc.* **8**, 564
Cato, B. T., Rönnäng, B. O., Rydbeck, O. E. H., Lewin, P. T., Yngvesson, K. S., Cardiasmenos, A. G., Shanley, J. F.: 1976, *Astrophys. J.* **208**, 87
Clark, B. G.: 1973, *Proc.* IEEE **61**, 1242
Cochran, W. D., Ostriker, J. P.: 1977, *Astrophys. J.* **211**, 392
Davidson, K., Harwit, M.: 1967, *Astrophys. J.* **148**, 443
De Jong, T.: 1973, *Astron. Astrophys.* **26**, 297
Dieter, N. H., Welch, W. J., Wright, M. C. H.: 1978 (in preparation)
Elmegreen, B. G., Lada, C. J.: 1977, *Astrophys. J.* **214**, 725
Forster, J. R., Welch, W. J., Wright, M. C. H.: 1977, *Astrophys. J.* **215**, L121
Forster, J. R., Welch, W. J., Wright, M. C. H., Baudry, A.: 1978, *Astrophys. J.* (in preparation)
Gatley, I., Becklin, E. E., Werner, M. W., Harper, D. A.: 1978, *Astrophys. J.* (in press)
Genzel, R., Downes, D., Bieging, J.: 1976, *Monthly Notices Roy. Astron. Soc.* **177**, 101 P
Genzel, R., Downes, D.: 1977a, *Astron. Astrophys.* **61**, 117
Genzel, R., Downes, D.: 1977b, *Astron. Astrophys. Suppl.* **30**, 145
Goldreich, P., Kwan, J.: 1974, *Astrophys. J.* **191**, 93
Hansen, S. S., Moran, J. M., Reid, M. J., Johnston, K. J., Spencer, J. H., Walker, R. C.: 1977, *Astrophys. J.* (in press)
Harris, S., Scott, P. F.: 1976, *Monthly Notices Roy. Astron. Soc.* **175**, 371
Harvey, P. J., Booth, R. S., Davies, R. D., Whillet, D. C. B., McLaughlin, W.: 1974, *Monthly Notices Roy. Astron. Soc.* **169**, 545
Haschick, A. D., Burke, B. F., Spencer, J. H.: 1977, *Science* (in press)
Israel, F. P.: 1977, *Astron. Astrophys.* **59**, 27
Johnston, K. J., Knowles, S. H., Sullivan, W. T., Moran, J. M., Burke, B. F., Lo, K. Y., Papa, D. C., Papadopoulos, G. D., Schwartz, P. R., Knight, C. A., Shapiro, I. I., Welch, W. J.: 1971, *Astrophys. J.* **166**, L21
Johnston, K. J., Knowles, S. H., Moran, J. M., Burke, B. F., Lo, K. Y., Papadopoulos, G. D., Read, R. B., Hardebeck, E. G.: 1977, *Astron. J.* **82**, 403
Kahn, F. D.: 1974, *Astron. Astrophys.* **37**, 149
Knowles, S. H., Johnston, K. J., Moran, J. M., Burke, B. F., Lo, K. Y., Papadopoulos, G. D.: 1974, *Astron. J.* **79**, 925
Kwan, J., Scoville, N.: 1976, *Astrophys. J.* **210**, L39
Little, L. T., White, G. J., Riley, P. W.: 1977, *Monthly Notices Roy. Astron. Soc.*, **180**, 639
Lo, K. Y., Burke, B. F., Haschick, A. D.: 1975, *Astrophys. J.* **202**, 81
Mader, G. L., Johnston, K. J., Moran, J. M., Knowles, S. H., Mango, S. A., Schwartz, P. R., Waltman, W. B.: 1975, *Astrophys. J.* **200**, L111
Mader, G. L., Johnston, K. J., Moran, J. M.: 1977, *Astrophys. J.* (in press)
Martin, A. H. M.: 1972, *Monthly Notices Roy. Astron. Soc.* **157**, 31
Martin, A. H. M., Gull, S. F.: 1976, *Monthly Notices Roy. Astron. Soc.* **175**, 235
Moran, J. M., Papadopoulos, G. D., Burke, B. F., Lo, K. Y., Schwartz, P. R., Thacker, D. L., Johnston, K. J., Knowles, S. H., Reisz, A. C., Shapiro, I. I.: 1973, *Astrophys. J.* **185**, 535
Moran, J. M.: 1976, in *Methods of Experimental Physics*, Vol. **12**c, ed. M. L. Meeks, New York: Academic Press, p. 228
Moran, J. M., Johnston, K. J., Spencer, J. H., Schwartz, P. R.: 1977, *Astrophys. J.* **217**, 434
Moran, J. M., Walker, R. C., Burke, B. F., Lo, K. Y., Johnston, K. J.: 1978, *Astrophys. J.* (in preparation)
Norris, R. P.: 1977, Diploma Report, University of Manchester
Olnon, F. M.: 1977, Ph. D. Thesis, University of Leiden
Phillips, T. G., Huggins, P. J., Neugebauer, G., Werner, M. W.: 1977, *Astrophys. J.* (in press)
Rieke, G. H., Low, F. J., Kleinmann, D. E.: 1973, *Astrophys. J.* **186**, L7
Scott, P. F.: 1978 (in preparation)
Scoville, N.: 1977, Symposium on Giant Molecular Clouds, Gregynog, Wales, UK (in preparation)
Shmeld, I. K., Strelnitskii, V. S., Muzylev, V. V.: 1976, *Astron. Zh.* **53**, 728; *Soviet Astron.* **20**, 411
Strelnitskii, V. S., Syunyaev, R. A.: 1972, *Astron. Zh.* **49**, 704; *Soviet. Astron.* **16**, 579 (1973)
Strelnitskii, V. S.: 1974, *Usp. Fiz. Nauk.* **113**, 463; 1975 *Soviet Phys.-Uspekhi* **17**, 507
Sullivan, W. T.: 1973, *Astrophys. J. Suppl.* **25**, 393
Van Blerkom, D., Auer, L.: 1976, *Astrophys. J.* **204**, 775
Walker, R. C., Johnston, K. J., Burke, B. F., Spencer, J. H.: 1977, *Astrophys. J.* **211**, L135
Walker, R. C.: 1977, Ph. D. Thesis, Massachusetts Institute of Technology
Wannier, P. G., Phillips, T. G.: 1977, *Astrophys. J.* (in press)
Willner, S. P.: 1976, *Astrophys. J.* **206**, 728
Wink, J. E., Altenhoff, W. J., Webster, W. J.: 1975, *Astron. Astrophys.* **38**, 109
Wynn-Williams, C. G., Becklin, E. E.: 1974, *Publ. Astron. Soc. Pacific* **86**, 5
Wynn-Williams, C. G., Becklin, E. E., Neugebauer, G.: 1974, *Astrophys. J.* **187**, 473
Wynn-Williams, C. G.: 1976, *Observatory* **96**, 6
Wynn-Williams, C. G., Becklin, E. E., Matthews, K., Neugebauer, G., Werner, M. W.: 1977a, *Monthly Notices Roy. Astron. Soc.* (in press)
Wynn-Williams, C. G., Becklin, E. E., Forster, J. R., Matthews, K., Neugebauer, G., Welch, W. J., Wright, M. C. H.: 1977b, *Astrophys. J.* **221**, L89
Yorke, H. W., Krügel, E.: 1977, *Astron. Astrophys.* **54**, 183
Zuckerman, B., Kuiper, T. B. H., Rodriguez Kuiper, E. N.: 1976, *Astrophys. J.* **209**, L137